Phys. Med. Biol., 1983, Vol. 28, No. 6, 723–729. Printed in Great Britain

Scientific Note

Measurement of spin–lattice relaxation times in nuclear magnetic resonance imaging

I L Pykett†, B R Rosen†, F S Buonanno‡ and T J Brady†

Department of Radiology† and Neurology Service‡, Research Building, Room 501, Massachusetts General Hospital, Fruit Street, Boston, MA 02114, USA

Received 26 June 1982, in final form 12 January 1983

1. Introduction

The diagnostic utility of proton (^{1}H) nuclear magnetic resonance (NMR) imaging is greatly enhanced when the image intensity is weighted with proton relaxation time information. This is because of the very significant variations of the proton spin–lattice (T_1) and spin–spin (T_2) relaxation times among various normal and abnormal soft-tissue structures which have essentially similar proton densities (Koutcher *et al* 1978, Mallard *et al* 1980). There are several reasons why it is useful to separate the individual contributions of T_1 and T_2 to the NMR signal. Firstly, *in vivo* measurements of these inherent tissue parameters may provide a useful diagnostic index, and might ultimately provide a certain degree of tissue characterisation (Davis *et al* 1981). Secondly, proton density and relaxation time data help elucidate the underlying physicochemical phenomena responsible for image alteration in diverse disease states, and hence aid in the design of more sensitive imaging schemes. Thirdly, several design criteria for an NMR imaging instrument are intimately linked with the relaxation times of the object to be studied. Of these reasons, the second requires an especially precise determination of relaxation data. The following paragraphs indicate factors affecting the accuracy of such measurements (especially with respect to T_1 determination) and, specifically, the accuracy of one approach which has been used in our laboratory is assessed. In addition, a brief discussion pertaining to the validity of data obtained from biological material is presented.

2. T_1 measurement pulse sequences

In conventional NMR spectroscopy, there are several pulse techniques commonly used to measure T_1 (Farrar and Becker 1971). Of these, the saturation recovery (SR), inversion recovery (IR) and 'null' methods have been used most frequently. In SR, a train of equally spaced 90° pulses is applied to the sample. After a short time a steady-state situation is reached, and, providing $T_2 \ll T_1$, the signal strength $S(\tau)$ is given by the expression:

$$S(\tau) = S(\infty)\,[1 - \exp(-\tau/T_1)] \tag{1}$$

where τ is the common interpulse spacing. Pulse sequences of this generic class are used frequently in NMR imaging. If several images are obtained with different values of τ, an estimate for T_1 at each pixel may be made independently of the spin density.

The first published T_1 map (Pykett and Mansfield 1978) was obtained using such a sequence; the T_1 values were calculated by a least squares procedure from three original SR scans.

In inversion recovery, the net magnetisation in the sample is first inverted by applying a 180° pulse. During an interpulse interval spin–lattice relaxation occurs, and the magnitude of the longitudinal component of magnetisation extant at a time τ after the 180° pulse is determined by measuring the signal amplitude following a 90° 'read' pulse. In this case, $S(\tau)$ is given by:

$$S(\tau) = S(\infty)\,[1 - 2\exp(-\tau/T_1)]. \tag{2}$$

When $\tau = T_1 \ln 2$, $S(\tau) = 0$ and an approximate T_1 value for the sample may be estimated by determining the value of τ for which the FID amplitude is zero; this is the 'null' method.

Equation (2) is valid only if full spin–lattice relaxation is allowed to occur before repeating the 180°–90° pulse pair. A repetition interval of at least $5T_1$ is therefore required, after which time the longitudinal component of magnetisation will have returned to 0.99 $S(\infty)$. However, this requirement is rarely met in the imaging context, as the imaging time would be lengthened to an unacceptable degree. Nevertheless, equation (2) has apparently been used to calculate T_1 values (Edelstein *et al* 1980, Hutchison and Smith 1981) even though the asymptotic $S(\infty)$ ('proton density') images show considerably decreased intensity in regions which are typically characterised by high spin density and long T_1 (e.g., the cerebrospinal fluid (CSF) in the brain). In fact, the relatively short waiting periods allowed between measurements renders the pulse sequences more akin to the fast inversion recovery (FIR) method (Canet, Levy and Peat 1975). A more thorough calculation of the signal amplitudes expected for real imaging pulse sequences has been given by Young *et al* (1982), Redpath (1982) and Pykett *et al* (1983).

3. Methods and results

The imaging system used for the data presented below was designed and built by Technicare Corporation, Ohio, USA. It employs a four-coil, resistive, water-cooled electromagnet which routinely operates at a field strength of 0.147 T, corresponding to a proton resonance frequency of 6.26 MHz. For the true three-dimensional (3D) imaging (Lai and Lauterbur 1981) approach adopted here, short, broadband radio frequency (RF) pulses are applied to the sample and the signal is elicited using spin-echoes (Hahn 1950). The full sequence used for T_1 measurements is sketched in figure 1. The signal amplitude S_1 of the first ('proton density') echo is given by:

$$S_1(t_e, t_b) = S_1(0, \infty)\exp(-2t_e/T_2)\{1 - 2\exp[-(t_b - t_e)/T_1] + \exp(-t_b/T_1)\} \tag{3}$$

and for the second ('T_1-weighted') echo, the signal amplitude S_2 is:

$$S_2(t_e, \tau, t_a) = S_1(0, \infty)\exp(-2t_e/T_2)\{1 - 2\exp(-\tau/T_1) + 2\exp[-(t_a + \tau - t_e)/T_1] - \exp[-(t_a + \tau)/T_1]\}. \tag{4}$$

Note that we assume that the signal decays essentially to zero between successive RF pulses. In the imaging context, this is ensured by applying magnetic field gradients appropriately, thus precluding refocusing of the transverse magnetisation. For the imaging experiments reported here, the timing parameters were set as follows: t_a = 1 000 ms; t_b = 800 ms; t_e = 8.58 ms; τ = 400 ms.

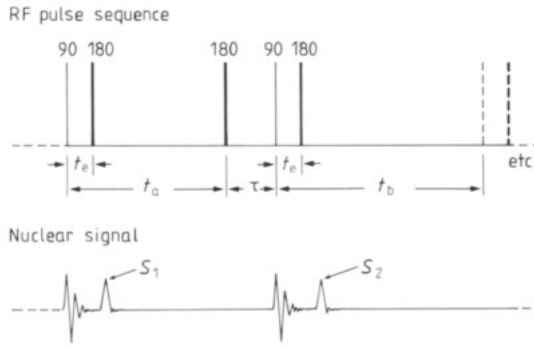

Figure 1. Radiofrequency pulse sequence used to generate the images of figure 2. The S_1 and S_2 spin echoes yield the approximate 'proton-density' and 'T_1-weighted' data sets.

Figure 2 shows selected images reconstructed from 3D data sets obtained using the above sequence on a normal volunteer. The total data accumulation time was 39.0 min. Figure 2(*a*) is the 'proton density' image; as expected, there is a considerably decreased intensity from the CSF of the lateral ventricles. Figure 2(*b*) is the 'T_1-weighted' image. Here, very good discrimination between grey and white matter is evident, as is usual with inversion recovery-type images. Since signals were elicited as spin-echoes, both images also have some degree of T_2-weighting. Figure 2(*c*) is a spin–lattice relaxation rate map. Here, areas of short T_1 (high relaxation rate) are shown brighter than areas of longer T_1.

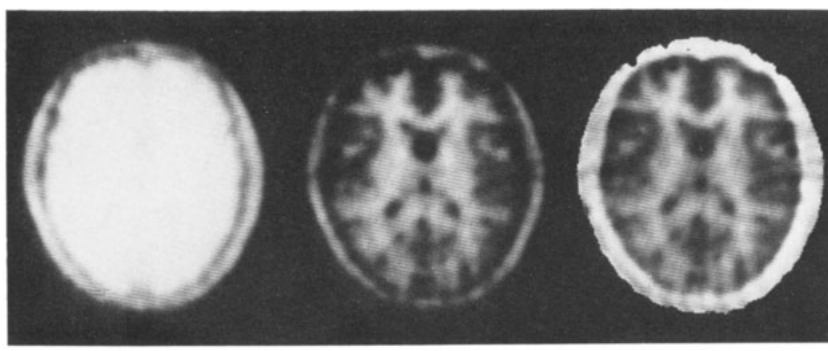

Figure 2. Approximate (*a*) 'proton-density' and (*b*) 'T_1-weighted' images derived from spin–echo signals generated by the pulse sequence of figure 1. The data were collected using a true, three-dimensional spatial encoding technique, and represent just one of an almost arbitrary number of possible plane orientations which may be reconstructed from the same raw data. (*c*) Is a relaxation rate image in which the brighter areas have shorter T_1 values.

As indicated earlier, equation (2) will give erroneous T_1 values when the pulse sequence of figure 1 is used; however, it is possible to calculate a correction function for the data using equations (3) and (4). A more convenient method is to refer to a computed look-up table in which the theoretically determined ratio S_2/S_1 is tabulated for various values of T_1, as determined using equations (3) and (4). The graphical form of such a look-up table is shown in figure 3 (solid line), calculated here for the

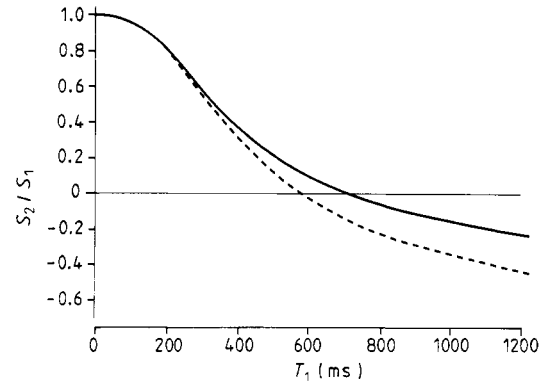

Figure 3. Graphical representation (solid curve) of the look-up table used to calculate T_1 values using equations (3) and (4). The following timing parameters were selected: $t_a = 1\,000$ ms, $t_e = 8.58$ ms, $\tau = 400$ ms. For comparison, the corresponding curve for equation (2) is shown (broken curve).

timing parameters listed above. For comparison the curve corresponding to equation (2) is plotted (broken line) where now $(S_2/S_1) = (S(\tau)/S(\infty))$. As expected, the curves become indistinguishable for short T_1. Note that the terms involving T_2 and $S_1(0, \infty)$ in equations (3) and (4) vanish when the ratio S_2/S_1 is calculated.

The validity of equations (3) and (4) was determined experimentally by measuring the signal amplitudes S_1 and S_2 obtained from various concentrations of copper sulphate and manganese chloride solutions. Firstly, accurate T_1 and T_2 relaxation times for each of ten (~200 cm^3) solutions (five $CuSO_4$, five $MnCl_2$) were determined on the imaging system, now operating in a 'spectrometer' mode, i.e., with no magnetic field gradients applied. For T_1 determinations, the standard IR pulse sequence was used, with eight appropriately chosen τ values. A delay time of at least $5T_1$ was allowed between repetition of the 180°–90° pulse pairs in order to ensure the validity of equation (2). For T_2 measurements, the method of Carr and Purcell as modified by Meiboom and Gill (1958) was used, again allowing at least $5T_1$ before sequence repetition. The relaxation time values thus obtained are shown in table 1. In addition, the relaxation rates ($1/T_1$ and $1/T_2$) are plotted against concentration of solution in figure 4. As expected, the points lie on a straight line.

Table 1. T_1 and T_2 values for copper sulphate and manganese chloride solutions at (21 ± 1) °C as determined by the traditional inversion recovery method (standard errors are quoted).

Concentration (mM)	T_1 (ms)		T_2 (ms)	
	$CuSO_4$	$MnCl_2$	$CuSO_4$	$MnCl_2$
0.5	832 ± 25	—	745 ± 11	—
1.0	461 ± 15	—	431 ± 6	—
2.0	274 ± 5	—	258 ± 4	—
3.5	171 ± 3	—	163 ± 3	—
5.0	129 ± 2	—	119 ± 2	—
0.1	—	524 ± 15	—	243 ± 4
0.2	—	309 ± 7	—	141 ± 3
0.3	—	202 ± 4	—	89.4 ± 2.0
0.5	—	133 ± 2	—	59.1 ± 1.0
1.0	—	67 ± 1	—	29.1 ± 0.8

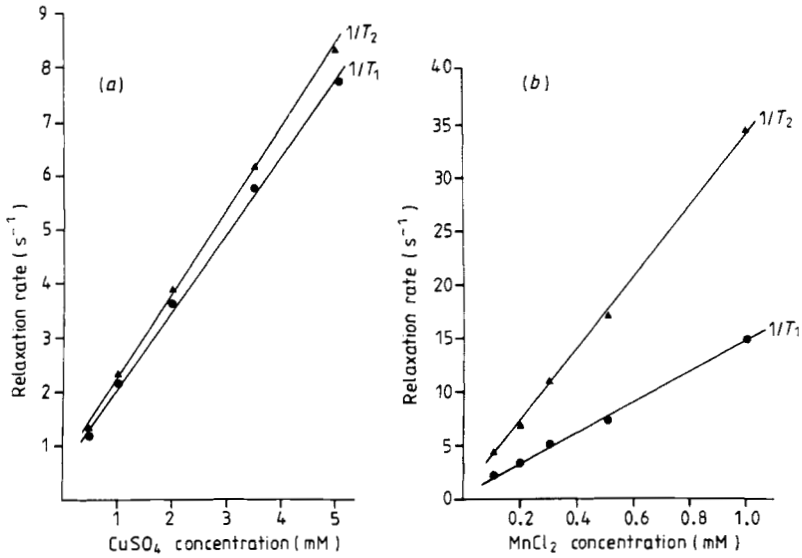

Figure 4. Relaxation rates ($1/T_1$ and $1/T_2$) against molar concentration for (a) standard copper sulphate and (b) manganese chloride solutions.

The signal amplitudes S_1 and S_2 were then measured for the same solutions using the pulse sequence of figure 1, and T_1 values determined using the look-up table. All measurements were made at (21 ± 1) °C. Figure 5 shows the T_1 values obtained experimentally using the traditional inversion recovery sequence, plotted against T_1 values obtained from the imaging (S_2/S_1) method. Over the T_1 range studied, the data points fit closely to the line of identity.

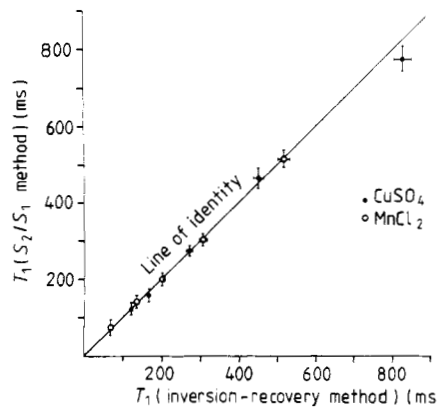

Figure 5. Spin–lattice relaxation times of copper sulphate and manganese chloride solutions, determined by the traditional inversion recovery pulse sequence, and by the imaging pulse sequence of figure 1. The straight line is the line of identity.

4. Discussion

The above data indicate that, using typical NMR imaging pulse sequences, accurate T_1 measurements can be made of simple, single-component systems when appropriate data analysis is employed. There is a significant error in T_1 values obtained using

equation (2) if the waiting interval between successive IR experiments is not sufficiently long. Such errors are clearly more severe for longer T_1 values. Optimisation of the precise timing parameters of the pulse sequences (Hanssum 1981) should enable sensitive and accurate measurements of T_1 in an imaging context. There are, however, several additional instrumental factors which must be taken into account. The above theory assumes ideal 90° and 180° pulses; in the case of imaging, there are at least three potential sources of spatially-dependent systematic error in the RF pulse angle due to non-uniform RF irradiation, and hence in reported relaxation time values. These errors can arise from (i) imperfect RF coil design, (ii) insufficient RF pulse bandwidth (in broadband pulse methods) and (iii) insufficient transmitter/receiver coil bandwidth. Non-linear amplifiers and other instrumental factors need also to be taken into account. In those methods which utilise selective pulses for plane selection purposes (Mansfield *et al* 1979) the RF pulse profile can introduce additional errors. In our 3D imaging method, selective pulses are not used.

With regard to interpretation of relaxation data obtained from biological samples, it is important to assess the validity of the results. As mentioned above, many tissues are known to exhibit multicomponent relaxation behavior, especially with respect to spin–spin relaxation (Pearson *et al* 1974, Fung and Puon 1981). Therefore, if only two images are used to determine the relaxation time, the computed value may be a function of the specific timing parameters of the RF pulse sequence, even though appropriate theoretical expressions may have been derived. The reported T_1 or T_2 value may then represent a weighted average of a family of values, which depend on the many different cellular microenvironments within which the signal-emitting nuclei are distributed. Multicomponent behavior may also be observed when the resolution element (pixel, sensitive volume, etc.), from which relaxation data is acquired, spans boundaries between tissues with different relaxation behavior. This is essentially a partial volume artefact. Another important consideration is the fact that flow or motion within the imaging volume may affect the measured T_1 values considerably; certainly the intensity distribution in the constituent images will be affected in a manner which depends on the flow direction and rate, pulse sequence, spatial encoding technique and other factors (Buonanno *et al* 1982a, Grant and Back 1982). A further consideration to bear in mind is the frequency and temperature dependence of relaxation times (Knispel *et al* 1974). Great care must therefore be exercised in the interpretation of T_1 and T_2 maps.

From a diagnostic point of view, pulse sequence parameters are frequently chosen to provide images which appear to have a high sensitivity for lesion detection. (It is unlikely, however, that all types of pathology will be detected optimally using a single pulse sequence.) In most cases, 'high sensitivity' would seem to correlate qualitatively with high contrast resolution, and several groups have presented images which demonstrate that a superior contrast resolution is obtained when inversion recovery type pulse methods, as opposed to saturation recovery techniques, are used (Young *et al* 1982, Buonanno *et al* 1982b, Pykett *et al* 1983). Furthermore, on theoretical grounds, the IR, and more especially the FIR sequences, can yield a more efficient determination of T_1 than the SR sequence (Becker *et al* 1980). Nonetheless, it has been suggested that SR images may be competitive in terms of contrast resolution if the pulse sequence parameters are chosen carefully (Edelstein *et al* 1982).

Pulse sequence requirements may well be different for qualitative rather than quantitative imaging. Many diagnoses are likely to be made quasi-subjectively from the visual appearance of an image. In this context, the steady-state free-precession

(SSFP) pulse sequence, for example (Hinshaw 1976), has provided very high quality images (Hawkes *et al* 1980, Buonanno *et al* 1982a); however, it is very difficult to separate the independent contributions from T_1 and T_2 in this case, and SSFP will therefore be of limited use for quantitative work.

Correlation of quantitative NMR tissue parameters determined at different institutions, possibly using diverse imaging systems, is a prerequisite for the establishment of a broad scientific data base. To this end, it behooves NMR imagers to render such measurements as free from systematic error or artefact as possible, and to be aware of the many factors affecting interpretation of results.

Acknowledgments

We acknowledge with thanks the many useful discussions held with the Massachusetts General Hospital NMR research group, and with Drs Waldo S Hinshaw, David M Kramer and Hong N Yeung. The secretarial and administrative assistance of DeeDee Correia, Edith Bell and Rita Zollo is sincerely appreciated. This work was supported in part by Technicare Corporation, Solon, Ohio, USA. T J Brady is the recipient of a Research Career Development Award from the National Cancer Institute.

References

Becker E D, Ferretti J A, Gupta R K and Weiss G H 1980 *J. Magn. Res.* **37** 381–94

Buonanno F S, Pykett I L, Kistler J P, Vielma J, Brady T J, Hinshaw W S, Goldman M R, Newhouse J H and Pohost G M 1982a *Radiology* **143** 187–93

Buonanno F S, Pykett I L, Brady T J, Black P, New P F J, Richardson E P, Hinshaw W S, Goldman M R, Pohost G M and Kistler J P 1982b *J. Comput. Assist. Tomogr.* **6** 529–35

Canet D, Levy G C and Peat I R 1975 *J. Magn. Res.* **18** 199–204

Davis P L, Kaufman L, Crooks L E and Margulis A R 1981 in *Nuclear Magnetic Resonance Imaging in Medicine* ed. L Kaufman, L E Crooks and A R Margulis (Tokyo: Igaku-Shoin) pp 71–100

Edelstein W A, Hutchison J M S, Johnson G and Redpath T 1980 *Phys. Med. Biol.* **25** 751–6

Edelstein W A, Bottomley P A, Hart H R, Leue W M, Smith L S, Schenck J F and Redington R W 1982 in *Proc. 1st Ann. Meeting, Soc. Magn. Res. in Med., Boston MA, August 1982.* (Soc. Mag. Res. in Med.) pp 52–3

Farrar T C and Becker E D 1971 *Pulse and Fourier Transform NMR—Introduction to Theory and Methods* (London: Academic Press) pp 20–2

Fung B M and Puon P S 1981 *Biophys. J.* **33** 27–37

Grant J P and Back C 1982 *Med. Phys.* **9** 188–93

Hahn E L 1950 *Phys. Rev.* **80** 580–94

Hanssum H 1981 *J. Magn. Res.* **45** 461–75

Hawkes R C, Holland G N, Moore W S and Worthington B S 1980 *J. Comput. Assist. Tomogr.* **4** 577–86

Hinshaw W S 1976 *J. Appl. Phys.* **47** 3709–21

Hutchison J M S and Smith F W 1981 in *Nuclear Magnetic Resonance Imaging in Medicine* ed. L Kaufman, L E Crooks and A R Margulis (Tokyo: Igaku-Shoin) pp 101–27

Knispel R R, Thompson R T and Pintar M M 1974 *J. Magn. Res.* **14** 44–51

Koutcher J A, Goldsmith M and Damadian R 1978 *Cancer* **41** 174–82

Lai C M and Lauterbur P C 1981 *Phys. Med. Biol.* **26** 851–6

Mallard J, Hutchison J M S, Edelstein W A, Ling C R, Foster M A and Johnson G 1980 *Phil. Trans. R. Soc. Lond.* **B289** 519–33

Mansfield P, Maudsley A A, Morris P G and Pykett I L 1979 *J. Magn. Res.* **33** 261–4

Meiboom S and Gill D 1958 *Rev. Sci. Instrum.* **29** 688–91

Pearson R T, Duff I D, Derbyshire W and Blanshard J M V 1974 *Biochim. Biophys. Acta* **362** 188–200

Pykett I L and Mansfield P 1978 *Phys. Med. Biol.* **23** 861–967

Pykett I L, Buonanno F S, Brady T J and Kistler J P 1983 *Stroke* **14** 173–7

Redpath T W 1982 *Phys. Med. Biol.* **27** 1057–65

Young I R *et al* 1982 *J. Comput. Assist. Tomogr.* **6** 1–18